



Research Article

Corrosion of stainless steel coated with a ZrO_2 film in a hydrogen sulfide gas environment



Lizhi Zhang¹ · Sansartuya Dorjpalam¹ · Guojun Ji¹  · Jingsi Peng¹

Received: 7 February 2020 / Accepted: 7 April 2020 / Published online: 16 April 2020
© Springer Nature Switzerland AG 2020

Abstract

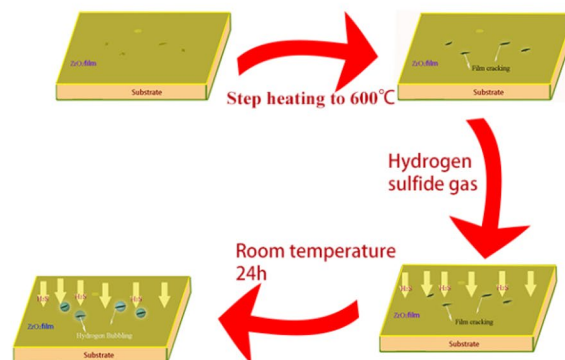
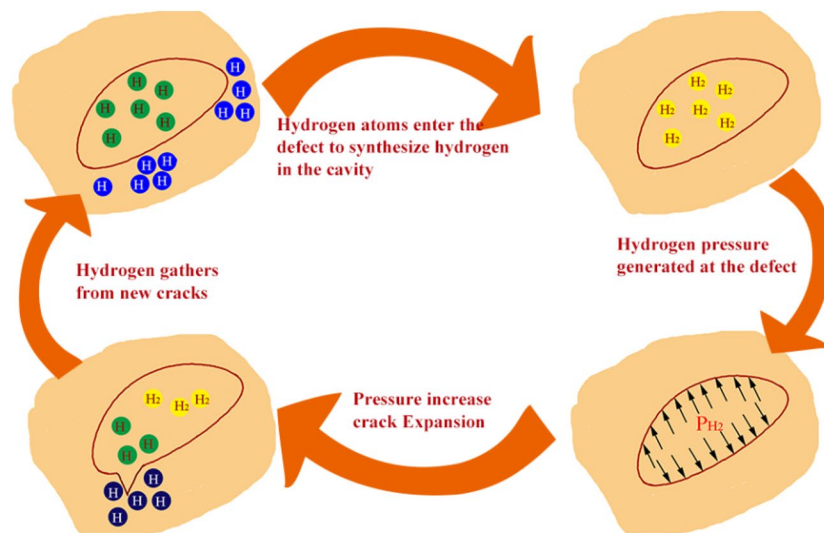
A zirconia sol was prepared by the sol–gel method and coated on the surface of stainless steel substrates. The gas corrosion test was carried out for the stainless steel substrates and for the coated samples using a high-temperature and high-pressure reactor. The coated samples and the substrates were placed in the reaction kettle, and it was filled with the H_2S gas at the pressures of 0.6, 0.8, and 1 MPa. After standing at room temperature for 24 h, the samples were observed by optical microscopy and a scanning electron microscopy, and it was found that as the pressure increases, the corrosion of the stainless steel substrates are more severe, while the film samples show only slight pitting corrosion. The experimental results show that in the corrosive H_2S gas environment, the stainless steel samples coated with the ZrO_2 film can effectively block the H_2S gas corrosion on the stainless steel substrate and reduce the hydrogen bubbling and hydrogen-induced cracking caused by gas corrosion. This finding has important practical significance for improving the service life of oil pipelines and reducing the occurrence of oil spills and other accidents.

✉ Guojun Ji, [jjgj@imut.edu.cn](mailto:jgj@imut.edu.cn) | ¹College of Chemical Engineering, Inner Mongolia University of Technology, Hohhot 010051, China.



SN Applied Sciences (2020) 2:915 | <https://doi.org/10.1007/s42452-020-2718-z>

Graphic abstract



Keywords ZrO₂film · H₂S · Hydrogen bubbling (HB) · Scanning electron microscope (SEM)

1 Introduction

Petroleum and natural gas are the mainstay of the current energy consumption and must be transported to energy shortage areas to alleviate the problem of energy shortage due to the uneven distribution of Petroleum and natural gas reserves [1]. Oil and gas transportation is a large problem, and in particular, gas in high-sulfur gas reservoirs containing H₂S is extremely corrosive to mining and transport equipment. Corrosion damage of oil and gas pipelines has become the main cause of many accidents. This makes pipeline, safety particularly important. Pipelines are another special mode of transportation that is

an alternative to the transport modes such as roads and shipping. Pipeline transportation has the advantages of continuity, stability, large transport capacity, convenient management and long-range transportation [2]. However, oil and natural gas contain sulfides that are highly unstable and decompose to produce H₂S gas. These sulfides are extremely corrosive to transportation pipelines. Currently, while corrosion-resistant alloy materials suitable for addressing H₂S corrosion are available, these materials are expensive, so that carbon steel is still the most commonly used material in pipelines [3]. There are many methods for protecting pipelines from corrosion. Among these, the use of anti-corrosion coatings is the most simple and

effective and is widely used. Stainless steel has become an ideal material, but stainless steel is susceptible to hydrogen sulfide gas corrosion. Study of the effect of zirconium oxide coatings on the corrosion resistance of steel 202 provides a basis for pipeline material selection.

ZrO₂ film is a coating material with great development potential, in both structural and functional materials [4]. Compared with other ceramic materials, it has high strength good wear resistance. ZrO₂ has excellent thermal and mechanical properties and a high coefficient of linear expansion that is close to that of the metal matrix [4, 5]. ZrO₂ has three phases: low-temperature monoclinic, medium-temperature tetragonal and high-temperature cubic phases, where the phase transition between the low-temperature monoclinic and medium-temperature tetragonal phases will result in a 3–5% (volume fraction) volume change and lead to the generation of microcracks. When the material is under stress, encountering these original microcracks during the main crack propagation process will bifurcate and change direction, thereby dispersing the energy of the main crack tip, increasing the fracture energy and enhancing the fracture. The transformation and toughening properties of zirconia make it one of the most important plastic ceramic materials; currently, in various metal oxide layers, the importance of ZrO₂ is second only to that of the alumina ceramics [6] used in many materials. Due to their high melting point and excellent corrosion resistance, ZrO₂ ceramics are becoming a very attractive alternative material for use in high-temperature applications [7].

Because of its excellent corrosion resistance, ZrO₂ has been made into nanocoatings and used in corrosive medium environments. Most studies have focused on the corrosion in a liquid environment, and ZrO₂ films have been rarely studied in gas corrosion experiments. Thus, experimental research is required to elucidate whether ZrO₂ film displays similarly excellent corrosion resistance requires in corrosive gas transport.

2 Materials and methods

2.1 Materials and sample preparation

The test samples are made of 202 stainless steel (chemical composition (wt%) C ≤ 0.15, Si ≤ 1.0, Mn ≤ 7.5–10.0, P ≤ 0.060, S ≤ 0.03, Ni 4.00–6.00, Cr 17.0–19.0, N ≤ 0.25). For corrosion test, 202 stainless steel was machined into specimens with the dimensions of 10 mm × 10 mm × 8 mm for corrosion test. All of the specimens were coated with epoxy, leaving an exposure area of 1 cm × 1 cm as the working surface. The high-pressure reactor was cleaned with absolute ethanol. The bare steel and film samples

were placed into the high-pressure reactor, and the reactor was filled with gaseous hydrogen sulfide (Purity 99%). The pressures of 0.6, 0.8, and 1 MPa were used, and the reaction was carried out at room temperature for 24 h prior to opening the vent valve.

2.2 Characterization

In this work, a zirconia sol was prepared by the sol–gel method. Zirconium oxide was coated on a 202 stainless steel substrate by the spincoating method, and the zirconia nanofilm was formed by stepwise heating to 600 °C [8]. The sintered zirconia powder was characterized by X-ray diffraction (XRD), and the surface roughness of the coated ZrO₂ film was observed with atomic force microscopy (AFM). The high-temperature and pressure reactor was used to simulate the required corrosion environment, and the coated samples were tested in gas corrosion experiments. Prior to the experiment, the bare steel samples and the coated samples were washed and dried with deionized water and absolute ethanol, and placed in the reaction kettle. The samples should be placed in a hanging position, not touching the inner wall of the kettle, so that a certain distance is retained between the samples. After filling with the hydrogen sulfide gas, the substrate samples and the film samples were moved after remaining at room temperature for 24 h and the microstructures of the samples after corrosion were examined using a metallographic microscope (ZYJ-330E, Shanghai Zhaoyi Optoelectronics Technology Co. Ltd.). The surfaces of the samples were further observed by scanning electron microscopy via a spectrometer (SEM, S-3400, Hitachi) and a field emission environment scanning electron microscope (FESEM, Quanta 650 FEG, USA) with Energy dispersive X-ray spectroscopy (EDS, EDAX Instruments) to detect the corrosion product components.

2.3 Analysis

ZrO₂ was coated on a stainless steel substrate and sintered at a high temperature of 600 °C to form a dense zirconia film. During the sintering process, ZrO₂ undergoes a phase transition. Figure 1 shows the XRD pattern of the zirconia xerogel at 600 °C, indicating that two zirconia crystal structures are present at this temperature, namely, the tetragonal phase (t-ZrO₂) and the monoclinic phase (m-ZrO₂). It is clear that ZrO₂ has mostly completed the transition from amorphous to crystalline. The surface morphologies of the samples coated with ZrO₂ film at a sintering temperature of 600 °C were observed by AFM. An examination of the AFM image (Fig. 2) shows that the ZrO₂ film of the coated samples is found in the shape of a sharp cone, and a few grid-like depressions are observed on the surface [9]. The

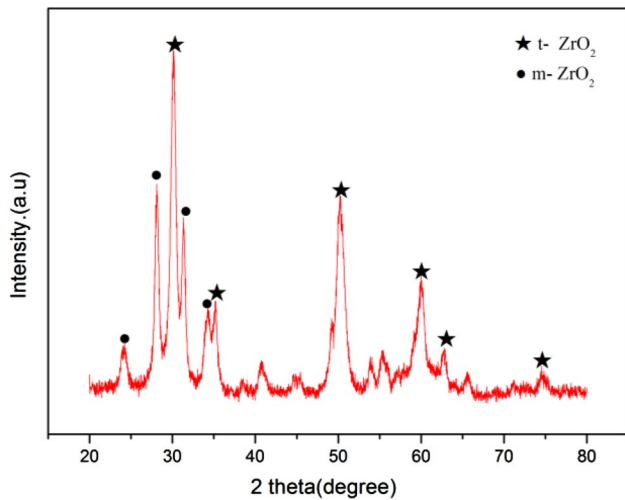


Fig. 1 XRD pattern of ZrO₂ xerogel at 600 °C sintering temperature

thickness of the film was measured by ellipsometer. The test results of five test points on the sample are shown in Table 1. As shown in the table, the average thickness of the film was 2058.31 Å.

The coated specimens and the stainless steel substrates were placed in a high-pressure reactor (upper connection pressure gauge), and the H₂S cylinder was connected to charge the H₂S gas to the pressures of 0.6, 0.8, and 1 MPa. After standing at room temperature for 24 h, the gas was released and the surface morphologies of the samples

were observed with a metallurgical microscope. Figures 3 and 4 show the surface morphology after the corrosion of the stainless steel substrates and the coated samples, respectively.

Figure 3a–c show the morphologies of stainless steel substrates, and Fig. 4a–c show the morphologies of coated samples. Images were taken immediately after the gas corrosion test, and the specimens were observed under a metallurgical microscope. The bubbles on the surface of the specimens were not broken, and the bubble morphology can be seen clearly observed. After a period of time, the bubble were broken and placed under a scanning electron microscope (3400 SEM, Japan). The bubbles morphologies are shown in Figs. 3d–f and 4d–f. The corrosion of the stainless steel matrix becomes more severe with the increase in the H₂S pressure, and cracks appear. When the H₂S pressure is 0.6 MPa, the gas causes significant corrosion to the stainless steel substrates, while the coated specimen (Fig. 2d) show essentially no bubbles. When the pressure is raised to 0.8 MPa, the number of bubbles significantly increased in the same unit area, and the substrate is severely corroded by the bubbles and starts to show the generation of cracks. At the same time, as observed from Fig. 1e, the bubble rupture gives rise to corrosion pits in the substrate, and some dark black tissue appears. The coated sample (Fig. 2e) showed only small gas bubbles in some areas. When the pressure rises to 1 MPa, the number of bubbles on the surface of the substrates increases, and the hydrogen sulfide bubbles become

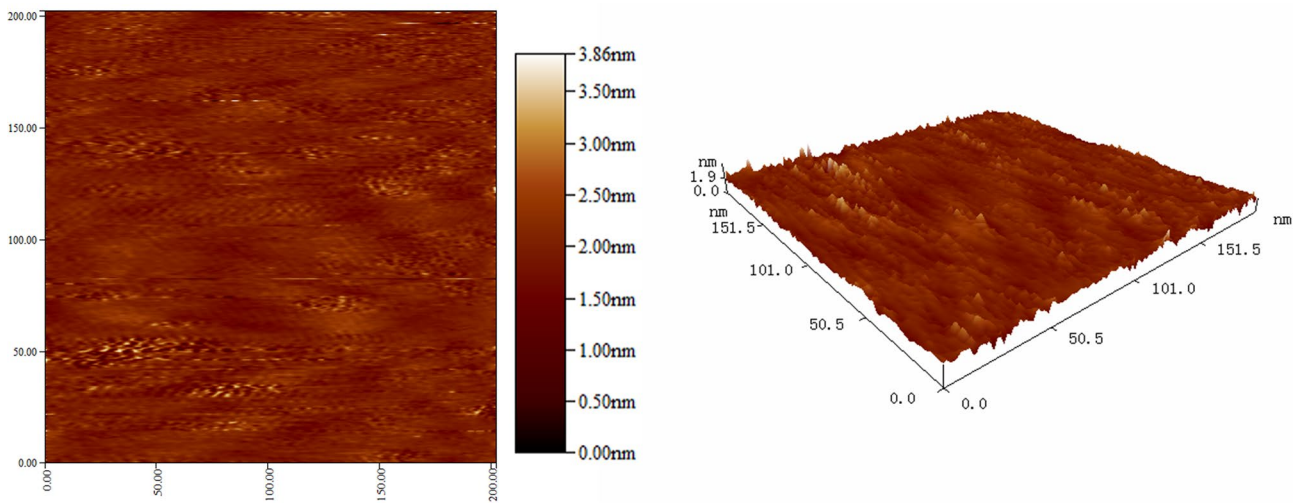


Fig. 2 Surface morphology of ZrO₂ film coated at 600 °C

Table 1 ZrO₂ film thickness (unit: Å)

	Point 1	Point 2	Point 3	Point 4	Point 5	Average
ZrO ₂ film	2056.71	2078.26	2054.77	2041.40	2060.39	2058.31

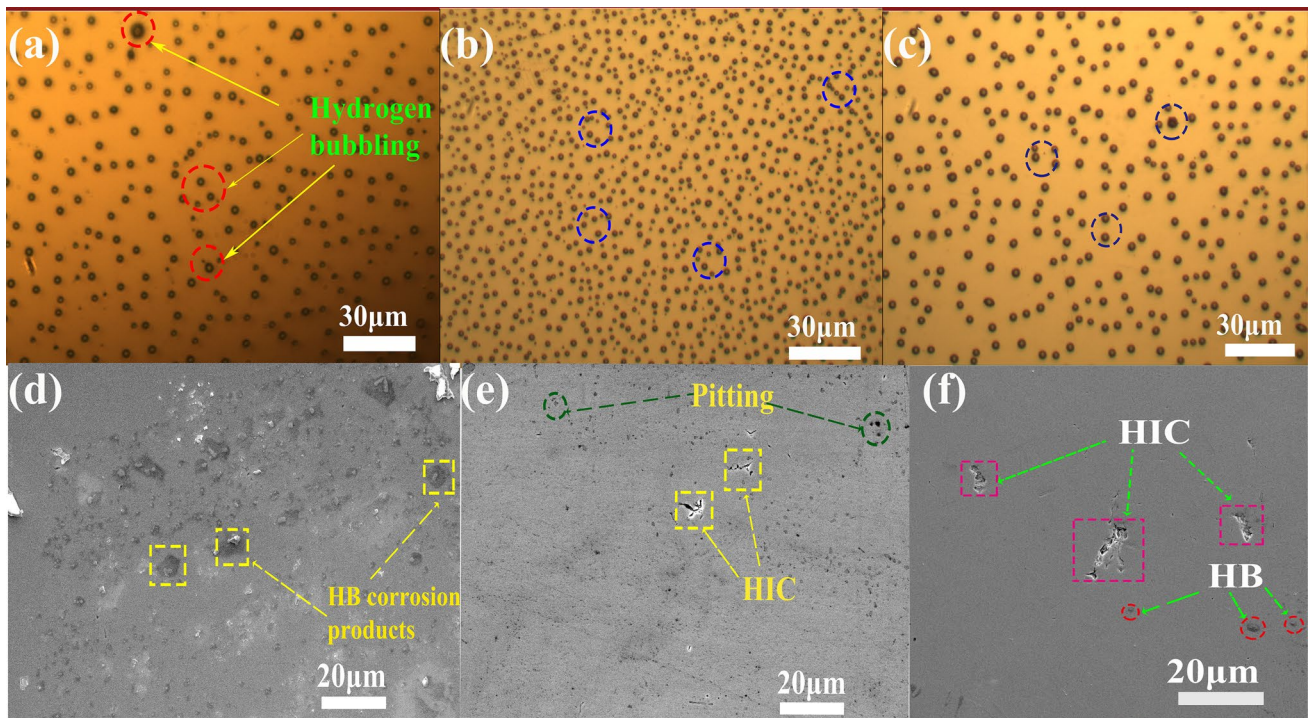


Fig. 3 Metallurgical microscope micrographs of the stainless steel samples and SEM micrographs of the stainless steel samples: **a, d** 0.6 MPa; **b, e** 0.8 MPa; **c, f** 1.0 MPa

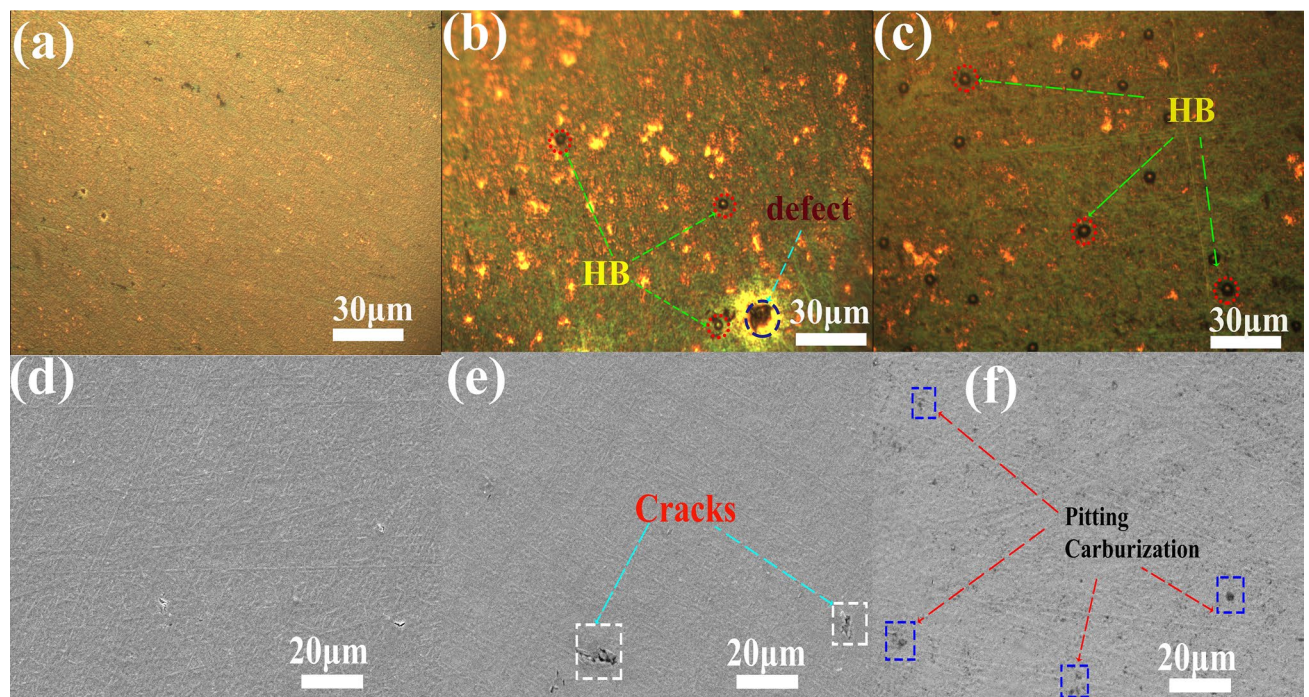


Fig. 4 Metallurgical microscope micrographs of the coated ZrO_2 film samples and SEM micrographs of the coated ZrO_2 film samples: **a, d** 0.6 MPa; **b, e** 0.8 MPa; **c, f** 1.0 MPa

connected, resulting in crack extension and expansion. The number of hydrogen bubbles in the coated samples (Fig. 2f) increases, and black corrosion spots appear on the surface. Hans-Arm and his team found that a large fraction of the H₂ produced by Fe and H₂S is adsorbed on the metal surface, reducing the likelihood of effective contact between the metal and H₂S, so that the reaction rate is gradually reduced, and this decrease favors adsorption to the metal. The amount of surface H₂ is reduced. After the two competing processes reach equilibrium, the corrosion is carried out at a certain speed. Therefore, the short-term experimental data cannot accurately reflect the long-term degree of corrosion. It is generally considered that the test results obtained after 50 or more hours are close to the actual value and can be used for the evaluation of long-term vulcanization corrosion [10].

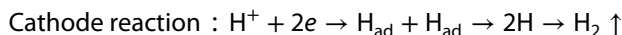
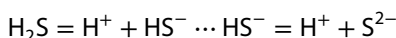
3 Result

3.1 Determination of the origin of the bubbling and the composition of the gas in the bubble

EDS characterization of the specimens was performed immediately after the corrosion test in order to determine whether the hydrogen sulfide gas gives rise to the bubbles. The EDS spectrum analysis is shown in Fig. 5, and it is observed that the bubble is not broken, and the elements of the selected area in the figure are detected. It is

clear that Sulfur was detected in bubbling area, and that hydrogen bubbling tears the metal. The dry H₂S gas has no corrosive effect on the metal matrix, while wet hydrogen sulfide will cause the corrosion of the metal matrix. In the wet hydrogen sulfide environment, hydrogen sulfide will ionize, making the water acidic, giving rise to the dissociation reaction of hydrogen sulfide in water:

The electrochemical corrosion process is described by: Ionization reaction of H₂S [11]:



Some of the H atoms produced by the cathode reaction diffuse into the steel, and the remaining H atoms generate the hydrogen adsorbed on the steel surface. The origin of the H₂S gas bubbling is as follows: when the hydrogen content is high, many materials will produce hydrogen bubbling or hydrogen-induced cracking in the absence of an external load [12–14]. The hydrogen atoms give rise to molecular hydrogen at the interface between the inclusion and the matrix or in a microporous cavity, resulting in high hydrogen pressure and microcracks. The expansion and connection of these microcracks leads to the formation of hydrogen bubbles or cracks. Hydrogen can only be combined into H₂ in a cavity of volume V to produce a hydrogen pressure given by $P = nRT/V$, where n is the number of moles of H₂ and T is the temperature. In the

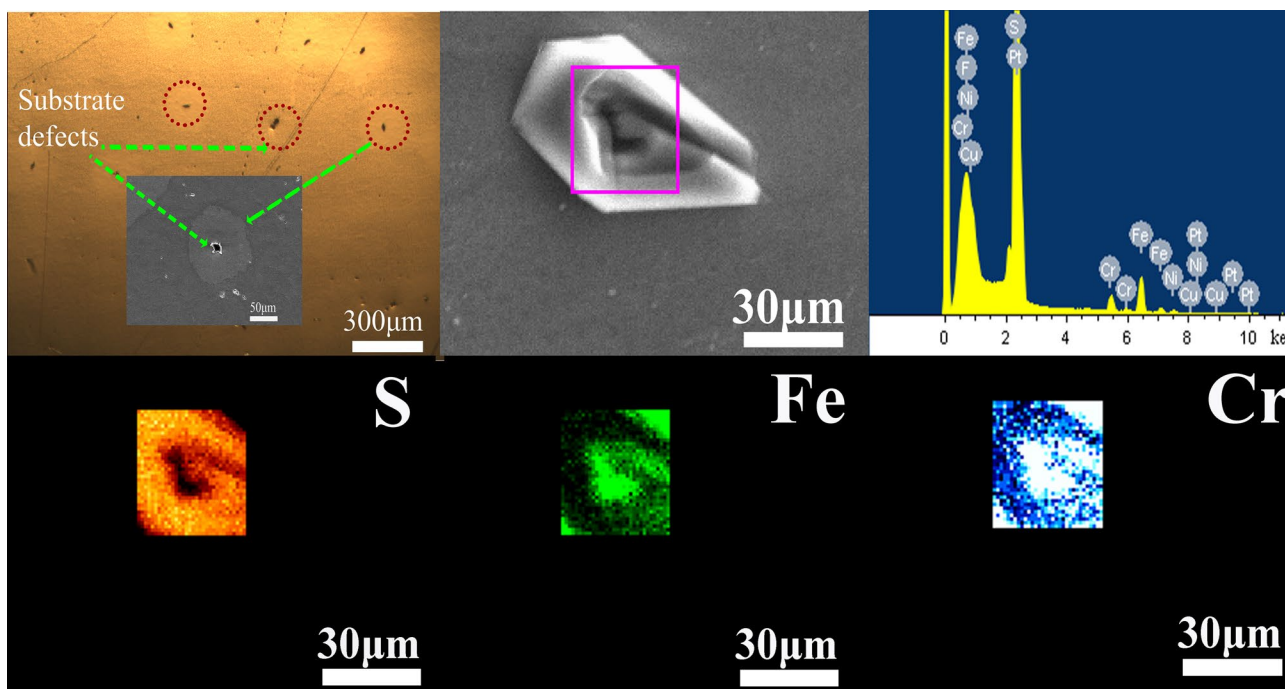
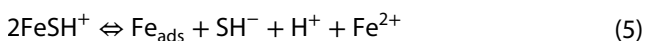
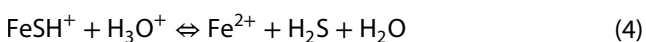
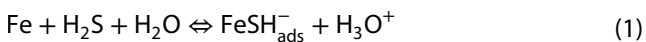


Fig. 5 Gas bubble EDS energy spectrum of stainless steel substrate under 1 Mpa hydrogen sulfide gas pressure

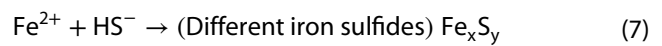
presence of micropores or microcracks in the material, hydrogen bubbles will be formed when hydrogen enters these defects [15]. Hydrogen bubbling occurs mainly at the surface defects and inclusions on the surface in the wet hydrogen sulfide environment. Electrochemical corrosion occurs on the inner wall of the pipeline, and hydrogen atoms with strong activity are generated by the cathodic reaction; these hydrogen atoms penetrate and diffuse into the steel and gather, precipitate and combine into hydrogen molecules at the defects and nonmetallic inclusions on the joint surface of the pipeline steel plate. Hydrogen accumulates and expands, increasing the internal pressure between the steel plate interface or the inclusion and the metal. When a certain hydrogen pressure is reached, the metal material will be torn off, giving rise to delamination defects [16].

As mentioned above, after the metal surface comes into contact with the corrosive medium, the corrosion reaction occurs, releasing hydrogen atoms. Moreover, H₂S can inhibit the escape of hydrogen atoms from these reactions and significantly increase the hydrogen atom concentration on the metal surface. Therefore, these hydrogen atoms will either combine into molecules or adsorb in the form of atoms on the metal surface. It is absorbed by the metal and promotes the formation of hydrogen bubbles. The presence of iron was not detected in the bubbling region, and a large amount of S was detected due to the adsorption of ionized sulfur ions on the surface.

Anode reactions: the dissolution of iron in acidic solution [17, 18]:



After the gas corrosion test of the film samples, water and some yellow–brown substances exist on the surface of the samples, and the samples undergo a series of electrochemical corrosion reactions. However, the high concentration of the iron ions at the material/medium interface will lead to another reaction that can form some insoluble iron sulfides on the metal surface in different forms. This reaction is described as:



The corrosion products (Fe_xS_y), which is the product of the electrochemical anode reaction after the bubble rupture, has a defective structure with poor adhesion to the steel surface, can easily fall off and oxidize, and has a positive potential. Therefore, as a cathode, corrosion products (Fe_xS_y) form an active micro battery with the steel substrate, and continue to corrode the steel substrate.

H₂S gas corrosion carbon steel proceeds via a complex reaction. The corrosion products vary with the corrosion environment. Mackinawite and cubic FeS are commonly observed corrosion products at normal temperature and low H₂S pressure [19]. Under high temperature and high H₂S pressure, troilite, pyrrhotite, pyrite, and other crystalline iron sulphide compounds may form [20]. While it was found by XRD analysis performed in research studies that the stainless steel corrosion products are nano crystals under the H₂S gas environment at 25 °C and are considered to be tetragonal pyrite as the only corrosion product [8]. The tetragonal pyrite(mackinawite) scale then dissolves in Fe(HS)⁺ and HS⁻, and Fe(HS)⁺ (Eqs. 5, 6) diffuses away from the metal surface. Finally, more H₂S reacts with the bare steel. This corrosion process continues to produce a very thin mackinawite layer, which repeatedly forms and dissolves [3, 21, 22].

Figure 5 shows that the stainless steel substrates have many surface defects such as inclusions, pores, and scratches. These defects will become hydrogen traps and provide a field for the formation of hydrogen bubbles that are considered to be responsible for degrading the mechanical properties and the performance of the metal [23–27]. Larger inclusions and pores correspond to larger hydrogen bubbling, making it easier for the metal to break. These inclusions were analyzed by EDS as nonmetallic inclusions, and the main components were found to be MnS and a small amount of Al₂O₃. The Mn content in the alloy will reduce the corrosion resistance of stainless steel, because Mn and S often form MnS inclusions in the microstructure of the alloy, and as the sulfur content increase, a larger amount of sulfide forms manganese sulfide and the unstable and easily dissolved MnS inclusions, leading to enhanced initiation of the corrosion at the interface of the inclusion matrix [28].

4 Discussion

Based on the results obtained for the corrosion surface, the anodic corrosion reaction is more likely to follow Eqs. (1)–(4) reaction formula. H₂S gas acts as a catalyst in the reaction. In the cathode reaction, some hydrogen atoms are reduced to hydrogen molecules, while others

are adsorbed on the surface together with sulfur ions, so a large amount of S is detected in the bubble.

ZrO₂ film sintered at 600 °C has many penetrating cracks in the coating. Organic components are completely decomposed and volatilized at 600 °C. The difference of thermal expansion coefficient between ZrO₂ coating and low carbon steel substrate will cause larger internal stress in the coating ($ZrO_2 \approx 12 \times 10^{-6}/^\circ C$, $\alpha_{Mild\ Steel} \approx 16 \times 10^{-6}/^\circ C$), eventually leading to cracks [29, 30]. When the matrix at the crack is exposed to hydrogen sulfide, hydrogen bubbles will be generated along the crack corrosion matrix, and the bubbles will lead to the separation the ZrO₂ film from the matrix. With the increase in the H₂S gas pressure, the bubble diameter and the number of bubbles formed at the crack increases continuously ZrO₂ can prevent corrosion by blocking the contact area between the gas and the stainless steel matrix. The gas can reach the surface of the matrix through the crack and corrode the stainless steel matrix. When the H₂S gas pressure increases to 0.8 MPa, hydrogen-induced cracking occurs on the surface of the test sample, and the hydrogen induced cracking corrosion mechanism is shown in Fig. 6. First, diffusion analysis is needed to simulate the absorption and transportation of hydrogen from the inner wall (in contact with the acidic environment) to the gap

point. The hydrogen distribution near the crack tip and the hydrogen flux of the crack flank can be obtained by analysis. The hydrogen distribution also controls the complex reaction of the hydrogen on the crack surface, thus affecting the formation mechanism of the pressure. The pressure in the crack can be determined by the current crack volume and the total mass of hydrogen molecules in the cavity. According to the stress level near the crack tip, when the hydrogen reacts, the fracture toughness of the steel is affected, thereby further advancing the HIC process. Finally, when the increase in the volume of the cavity is sufficiently large to give to a pressure drop, crack propagation is suppressed. The entire cycle is performed until the final conditions are reached (the predetermined amount of crack propagation is achieved) [31].

According to Fig. 7a, b, not only microcracks but also dark black structures at present on the surface of the coated samples. According to EDS analysis, these black areas contain high amounts of C and O and a very small amount of S. Some of these dark black materials are due to the precipitation of chromium carbide in the carburized layer when the stainless steel temperature exceeds 540 °C, not only reducing the free chromium content on the stainless steel surface but also making the original single austenite phase of stainless steel become a multiphase

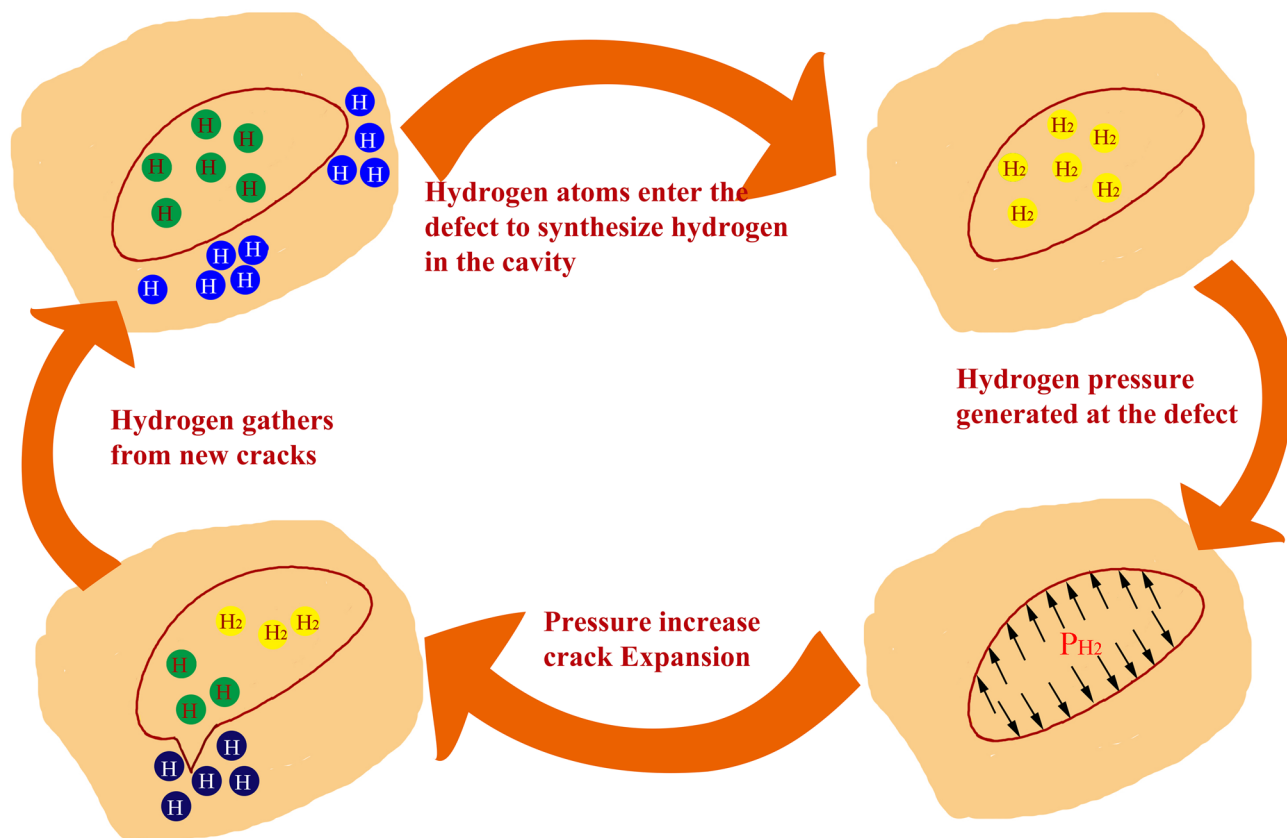


Fig. 6 Schematic diagram of hydrogen induced cracking mechanism

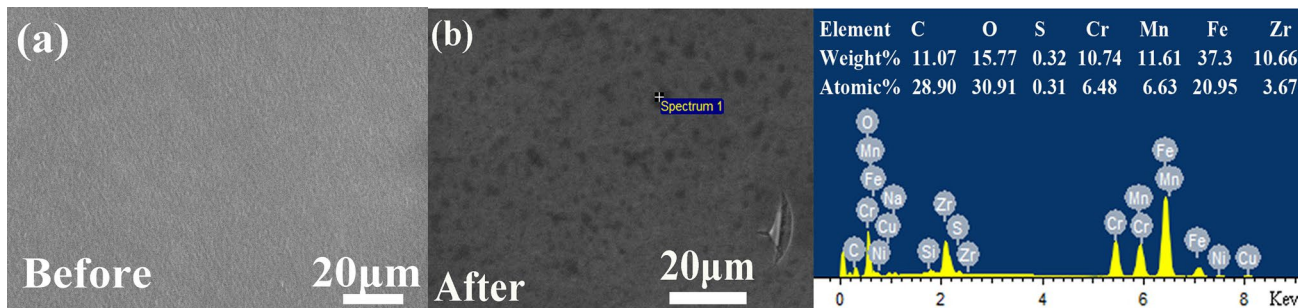


Fig. 7 Morphology of the coated specimen before and after corrosion

weave with new phase formation, thus reducing the corrosion resistance of the stainless steel. This is the reason for the appearance of the dark black tissue [32]. There are still some black spots that did not appear prior to the corrosion. This is because these black spots are caused by the H₂S gas. When the H₂S gas pressure increased to 1 MPa, black substances appeared on the ZrO₂ film surface. Therefore, the coated sample was corroded, resulting in corrosion points. The ZrO₂ thin film is a porous ceramic thin film. Although it can prevent the outward diffusion

of Fe, Mn and the inward diffusion of O to some extent, due to the presence of pores and cracks in the thin film, the samples coated with the ZrO₂ thin film often form an oxide film, usually Fe₂O₃ and Cr₂O₃ between the bonding layer and the surface ZrO₂ coating after high-temperature sintering. Additionally, Fe₂O₃ and Cr₂O₃ provide conditions and places for H₂S gas corrosion [27].

Figure 8 shows the hydrogen bubble morphology and EDS elemental analysis of a sample coated with aZrO₂ film. It observed from the SEM image that the hydrogen

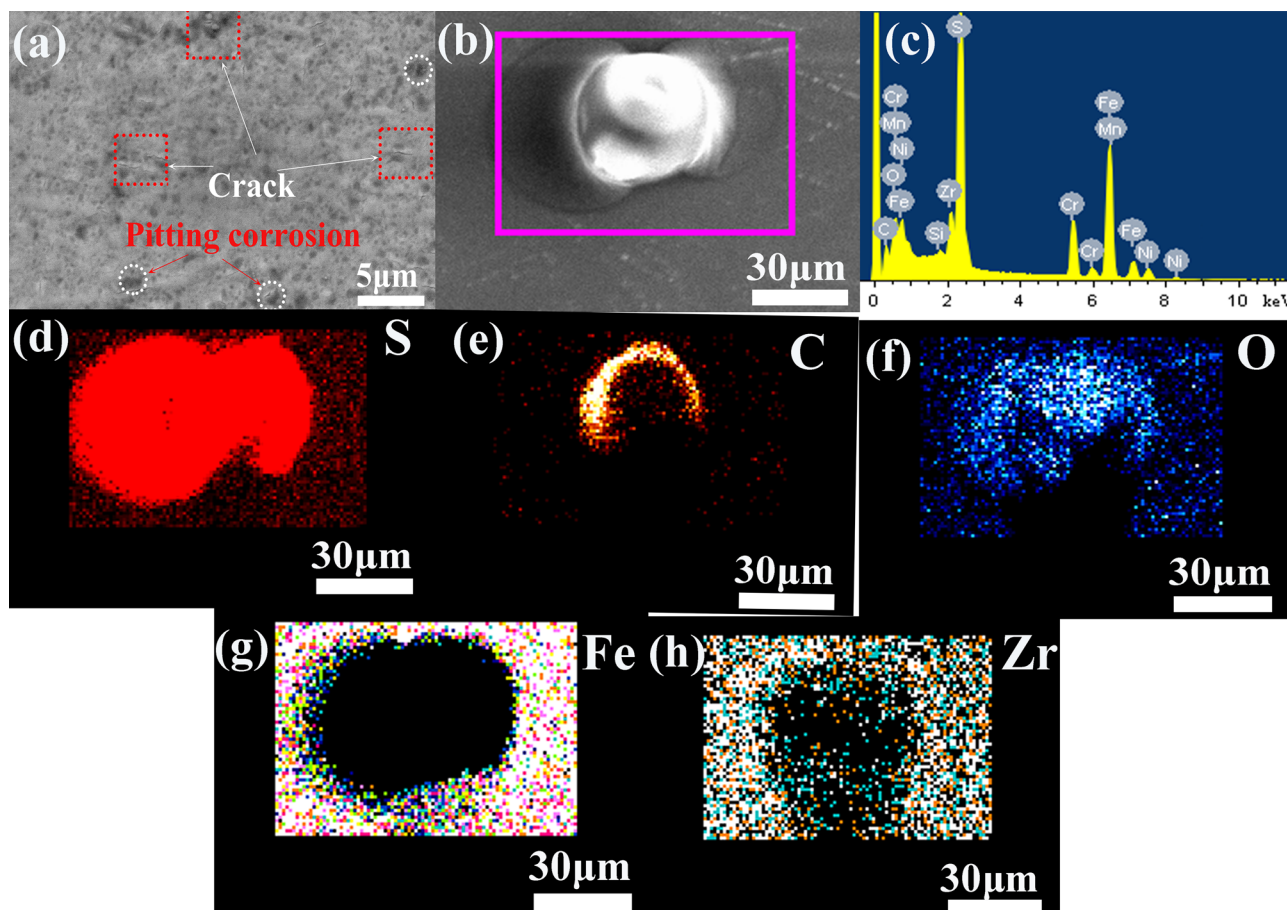


Fig. 8 Gas bubble EDS energy spectrum of coated samples under 1 Mpa hydrogen sulfide gas pressure

bubbling is located at the position of the crack, showing the bubbling from elemental analysis. There is no distribution of elements such as Fe, Cr, and Zr (Fig. 9h, i), and the element S, C and O (Fig. 9e–g) are detected in the edge region of the bubble, and the oxide in the ZrO_2 film is excessive during the sintering process. Growth causes significant internal stresses that cause the film to rupture, and the substrate at the cracks oxidizes at high temperatures [33]. C and O only appear in the rupture or bubbling of the film. C and O are not detected around the matrix bubbling. Only two elements are detected in the hydrogen bubbling of the coated samples. It is further observed from the energy spectrum presented in Fig. 8 that Fe and Cr carbides and oxides are not formed, So C and O originally existed in the coated sample.

Through EDS spectrum analysis, it was determined that the film rupture is caused by the entry of the hydrogen sulfide gas. Figure 9 shows the energy spectrum scanning analysis of the sample coated with the ZrO_2 film. It is clearly observed from the scanning results that sulfur is present in the rupture zone while zirconium is absent. The hydrogen sulfide gas enters the ZrO_2 film through the defects in the substrate and in the film to generate hydrogen bubbling, and the zirconia film no longer protects the substrate after the rupture. The ZrO_2 film often generates microcracks due to the phase transition between the low-temperature monoclinic and mesothermal tetragonal phases. While this phenomenon is unavoidable, the microcracks produced

by the phase transformation have no effect on the corrosion. This is observed from Fig. 9. While S was detected in the rupture zone, it was not detected in the other areas of the coating, indicating that the zirconia film can effectively hinder the corrosion of the stainless steel substrate by the H_2S gas.

5 Conclusions

The gas corrosion of the coated specimens and stainless steel matrices has been investigated in this work. The main conclusions are as follows:

- (1) Under the pressures of 0.6, 0.8 and 1 MPa, corrosion of the metal surface becomes increasingly severe with the increase in the pressure. In the absence of external stress, the hydrogen damage on the metal surface caused by the H_2S gas is mainly manifested as hydrogen bubbles and hydrogen-induced cracking, which leads to tearing of the metal surface and causes irreparable corrosion damage.
- (2) When the H_2S gas pressure is lower than 0.6 MPa, there is essentially no corrosion effect on the surface of the coated sample, while the surface of the stainless steel substrate shows significant hydrogen bubbling.

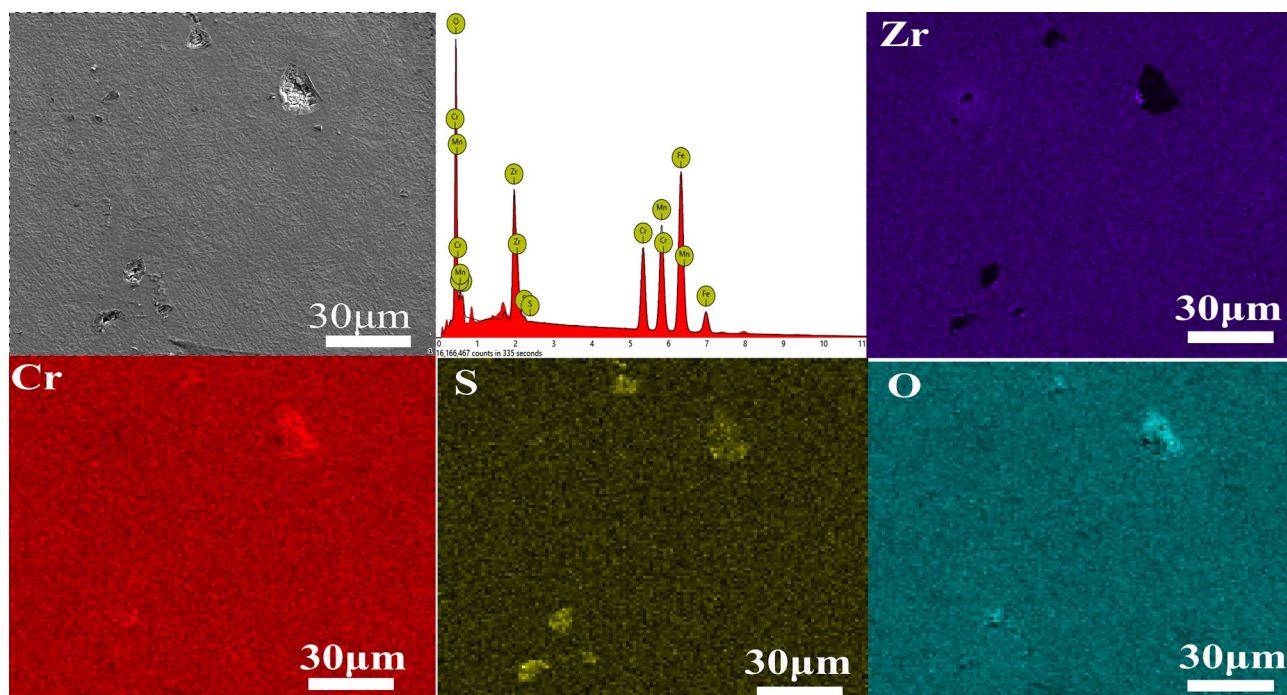


Fig. 9 Surface morphology and EDS spectrum of laminating samples under 1 Mpa H_2S gas

- (3) When the pressure rises to 0.8 MPa, hydrogen bubbles accompanied by cracks are observed on the surface of the substrate. A small number of hydrogen bubbles appear in some areas of the surface of the coated sample.
- (4) When the pressure rises to 1 MPa, the hydrogen bubbles on the surface of the matrix are dense, the matrix metal tears, the cracks increase, and the cracks propagate along the transverse and longitudinal directions. The number of hydrogen bubbles on the surface of the coated samples increased, but no cracks were observed.

In conclusion, ZrO₂ film coating on stainless steel substrates effectively prevents hydrogen bubbles and hydrogen-induced cracking caused by H₂S gas corrosion and greatly reduces the corrosion of metal substrates by the corrosive gas.

Acknowledgements The authors would like to acknowledge the financial support from the Natural Science Foundation of Inner Mongolia Autonomous Region of China (2019MS01016).

Compliance with ethical standards

Conflict of interest The authors declared that they have no conflicts of interest to this work. We declare that we do not have any commercial or associative interest that represents a conflict of interest in connection with the work submitted.

References

1. Mohtadi-Bonab MA, Eskandarib M (2017) A focus on different factors affecting hydrogen induced cracking in oil and natural gas pipeline steel. *Eng Fail Anal* 79:351–360
2. Badida P, Balasubramaniam Y, Jayaprakash J (2019) Risk evaluation of oil and natural gas pipelines due to natural hazards using fuzzy fault tree analysis. *J Nat Gas Sci Eng* 66:284–292
3. Wen XL, Bai PP, Luo BW, Zheng SQ, Chen CF (2018) Review of recent progress in the study of corrosion products of steels in a hydrogen sulphide environment. *Corros Sci* 139:124–140
4. Liang B, Chen H (2003) Application and research of zirconia coating (thin film). *B Chin Ceram soc* 22:63–67
5. Wang H, Zeng LK, Wu JQ, Yin H (2000) Current status and prospects of research on surface modification technology of ceramic materials. *Mater Prot* 33:44–46
6. Run H, Dou MM, Li HP (2000) Phase transformation toughening mechanism and application of zirconia ceramics. *J Ceram* 01:46–50
7. Bocanegra-Bernal M, Díaz de la Torre S (2002) Phase transitions in zirconium dioxide and related materials for high performance engineering ceramics. *J Mater Sci* 37:4947–4971
8. Bai PP, Zheng SQ, Zhao H, Ding Y, Wu J, Chen CF (2014) Investigations of the diverse corrosion products on steel in a hydrogen sulfide environment. *Corros Sci* 87:397–406
9. Zhang W, Ji GJ, Bu AM, Zhang B (2015) Corrosion and tribological behavior of ZrO₂ films prepared on stainless steel surface by the Sol–Gel method. *ACS Appl Mater Interfaces* 7:28264–28272
10. Hans A, Paul D, Charles H et al (1960) Mechanism of the iron-hydrogen sulfide reaction at elevated temperature. *J Electrochem Soc* 10:7264
11. Ogundele GI, White WE (2012) Some observations on the corrosion of carbon steel in sour gas environments: effects of H₂S and H₂S/CO₂/CH₄/C₃H₈ mixtures. *Corrosion*. 42:398–408
12. Yen SK, Huang IB (2003) Critical hydrogen concentration for hydrogen-induced blistering on AISI 430 stainless steel. *Mater Chem Phys* 80:662–664
13. Tetelman AS, Robertson WD (1963) Direct observation and analysis of crack propagation in iron-3% silicon single crystals. *Acta Metall* 11:415–425
14. Ren XC, Shan GB, Yan WY, Su YJ, Gao KW, Li JX (2005) Nucleation, growth and cracking of hydrogen bubbling. *Chin Sci Bull* 50:1689–1692
15. Ren XC, Zhou QJ, Qi WY, Su YJ, Li JX, Qiao LJ (2007) Mechanism of hydrogen bubbling nucleation in metals. *Chin Sci Bull* 52:725–729
16. Zhang QM, Xu CB, Chen MB (2013) Mechanism analysis of bubbling delamination defects in gas pipelines in service. *Oil Gas Field Surf* 32:38–39
17. Cheng XL, Ma HY, Zhang JP, Chen X, Chen SH, Yang HQ (1998) Corrosion of iron in acid solutions with hydrogen sulfide. *Corrosion* 54:369–376
18. Lucio-Garcia MA, Gonzalez-Rodriguez JG, Casales M, Martinez L, Chacon-Nava JG, Neri-Flores MA, Martinez-Villafa A (2009) Effect of heat treatment on H₂S corrosion of a micro-alloyed C-Mn steel. *Corros Sci* 51:2380–2386
19. Sardisco JB, Wright WB, Greco EC (1963) Corrosion of iron in on H₂S-CO₂-H₂O system: corrosion film properties on pure iron. *Corrosion* 19:354–359
20. Smith SN, Joosten MW (2015) Corrosion of carbon steel by H₂S in CO₂ containing oilfield environments-10 year update. NACE International, Houston
21. Sun W (2006) Kinetics of iron carbonate and iron sulfide scale formation in CO₂/H₂S corrosion, PhD Thesis, Ohio University.
22. Marcus P, Protopopoff E (1990) Potential-pH diagrams for adsorbed species. Application to sulfur adsorbed on iron in water at 25 °C and 300 °C. *J Electrochem Soc* 137:2709–2712
23. Roth J, Schmid K (2011) Hydrogen in tungsten as plasma-facing material. *Phys Scr T* 145:014031
24. Tanabe T (2014) Review of hydrogen retention in tungsten. *Phys Scripta* 2014(T159):014044
25. Gao L, Jacob W, von Toussaint U, Manhard A, Balden M, Schmid K, Schwarz-Selinger T (2017) Deuterium supersaturation in low-energy plasma-loaded Tungsten surfaces. *Nucl Fusion* 57:016026
26. Sang CF, Sun JZ, Bonnin X, Liu SG, Wang DZ (2013) Numerical simulation of the bubble growth due to Hydrogen isotopes inventory processes in plasma-irradiated tungsten. *J Nucl Mater* 443:403–408
27. Hu X, Koyanagi T, Fukuda M, Kiran Kumar NAP, Snead LL, Wirth BD, Katoh Y (2016) Irradiation hardening of pure tungsten exposed to Neutron irradiation. *J Nucl Mater* 480:235–243
28. Yu J, Ji GJ, Shi ZM, Wang XH (2019) Corrosion resistance of ZrO₂ films under different humidity coal gas conditions at high temperature. *J Alloy Compd* 783:371–378
29. Mei LF, Liang KM (2002) Study on oxidation protection of low carbon steel by zirconium dioxide coating prepared by sol-gel method. *Rare Metal Mater Eng* 31:92–95

30. Li HB, Liang KM, Mei LF, Gu SR (2002) Protection of corrosion of low carbon steel by ZrO₂ coating prepared by sol-gel method. *Corros Sci Prot* 14:92–94
31. Traidia A, Alfano M, Lubineau G, Duval S, Sherik A (2012) An effective finite element model for the prediction of hydrogen induced cracking in steel pipelines. *Int J Hydrogen Energy* 37:16214–16230
32. Zhou MF, Zhao C (2017) Influence of low temperature ion-gas carburizing temperature on carburized layer of AISI 316L austenitic stainless steel. *Heat Treat Met* 42:75–79
33. Tian XW, Wang BJ, Liu SF, Huang BX (2018) High temperature oxidation behavior of 310S austenitic stainless steel wire. *Hot Process Technol* 47:51–58

Publisher's Note Springer Nature remains neutral with regard to jurisdictional claims in published maps and institutional affiliations.